Multipole approach to orientational interactions in solid C_{60}

T. Yildirim, A. B. Harris, and S. C. Erwin
Department of Physics, University of Pennsylvania, Philadelphia, Pennsylvania 19104

M. R. Pederson
Complex Systems Theory Branch, Naval Research Laboratory, Washington, D.C. 20375-5000
(23 October 1992; revised manuscript received 8 February 1993)

We calculate electrostatic multipole moments of C_{60} up to $l = 18$ using the quantum-mechanical charge distribution with icosahedral symmetry obtained from *ab initio* calculations. It is found that the second nonzero moment ($l = 10$) is comparable to the first nonzero moment ($l = 6$). The values of several low-order multipole moments are almost ten times smaller than those found from the charge distribution of recently proposed potential models and thus the actual Coulomb interaction between C_{60} is much smaller than previously predicted. Much better agreement with calculated multipoles is obtained from a model which introduces point charges at the center of hexagonal and pentagonal plaquettes, following the physical arguments of David *et al.* [Nature **353**, 147 (1991)]. We show that a multipole expansion including only $l = 6$ and 10 moments can predict the potential due to a molecule at distances $R \geq 2R_0$ within an error of about 5%, where R_0 is the radius of the C_{60} molecule. At distances less than $R < \frac{3}{2}R_0$ the multipole expansion is qualitatively incorrect even if one includes the terms up to $l = 18$, indicating the importance of short-range quantum effects at these distances. The Coulomb interaction we obtain predicts two nearly degenerate, locally stable configurations for solid C_{60}: (1) a metastable structure with Pa3 symmetry and setting angle $\phi = 23.3°$, close to experimentally observed value, and (2) a global minimum with the Pa3 structure but a setting angle $\phi = 93.6°$. We give physical arguments for expecting two such configurations and give a qualitative explanation for their near degeneracy. We conclude that a satisfactory intermolecular potential requires a first-principles calculation of the quantum-mechanical short-range repulsive interactions.

I. INTRODUCTION

Solid C_{60} is a system that is interesting for both theoretical and technological reasons. The metal-doped systems, such as K_3C_{60}, are moderately high-temperature superconductors,[1] whereas undoped C_{60} shows an orientational ordering transition. This paper is concerned with the quantum-mechanical basis for models of orientational interactions between C_{60} molecules.

Before discussing the orientational properties of solid C_{60}, we briefly review some properties of the isolated molecule. The C_{60} molecule is a nearly spherical molecule in the shape of a truncated icosahedron. (For a description of icosahedra see Ref. 2). The C_{60} truncated icosahedra thus represent a replica, on an atomic scale, of a soccer ball, as pictured in Ref. 3. The molecule has 20 hexagonal and 12 pentagonal faces. The pentagons are regular (i.e., all sides are equal), whereas the hexagons consist of alternate single and double bonds having respective lengths of 1.45 Å and 1.40 Å.[4,5] For some purposes, e.g., where only symmetry is important, it is convenient to consider the simpler untruncated icosahedron having 12 vertices and 20 faces. When circumscribed by a cube such that each face of the cube has a twofold axis passing through its center, one obtains the schematic representation shown in Fig. 1(a). This orientation is referred to as the "standard" orientation.

The orientational properties of solid crystalline C_{60} are unique and quite interesting. This solid undergoes a phase transition[6] from a high-temperature orientationally disordered phase[7] to a low-temperature orientationally ordered phase[6] whose structure is that of space group Pa3.[8–11] In this structure each of the four molecules in the unit cell is rotated about its local [1,1,1] direction, starting from the standard orientation, through a setting angle ϕ, whose value is about 22°–26°.[8–11] (The symmetry and description of this structure is discussed in detail in Ref. 12.) Although the nature of the Landau theory to describe this transition was first obtained[12] on the basis of symmetry alone, it is of course interesting to give a statistical treatment of this transition[13] and other orientational properties[14,15] starting from a microscopic orientational Hamiltonian.

Clearly, to understand many of the properties of C_{60} and its derivatives, it is essential to have a good intermolecular potential. In many contexts such a potential may be viewed as consisting of two parts: one the isotropic (orientation-independent) part and the other the orientation-dependent part. The description of the dynamics of the center of mass of the molecules[14,15] depends mainly on the isotropic part, whereas orientational dynamics of the molecules depends mainly on the orientational-dependent part of the intermolecular potential,[14,15] which is more sensitive to the model chosen. A reasonable orientational potential must be consistent with the stability of the observed Pa3

0163-1829/93/48(3)/1888(11)/$06.00

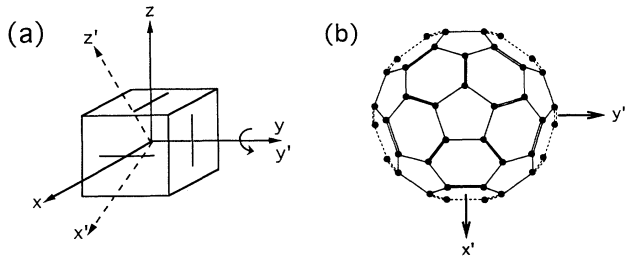

FIG. 1. Two different orientations of C_{60}. (a) Shown here is an icosahedron inscribed in a cube. Only the edges of the icosahedron which lie in the faces of the cube are shown. The 12 vertices of the icosahedron are located at ends of the edges which lie in the faces of the cube. For the truncated icosahedron, i.e., for C_{60}, each vertex of the icosahedron is flattened into a pentagon (Refs. 2 and 12). In this orientation the x, y, and z axes are twofold axes. The primed coordinate system (in which the z' axis is a fivefold axis) is obtained by rotation through an angle $\theta \sim 31.72°$ about the y axis. (b) Projection onto the x'-y'axis of C_{60} when the z' axis coincides with a fivefold symmetry axis (whose positive direction is out of the page). Note that the x'-z' plane is a mirror plane. Multipole moments are specified in this prime coordinate system.

structure.[8,10,11] The early potentials relied on atom-atom Lennard-Jones potentials. Molecular-dynamics simulations using such potentials found that the orientationally ordered cubic structure was unstable to a tetragonal distortion.[16] It was then clear that better orientational potentials were required. By now two such improved intermolecular potentials have been proposed.[17,18] In both cases the isotropic part of the potential is well modeled by Lennard-Jones potentials taken from graphite. However, to stabilize the observed Pa3 structure, both groups introduced charges on the single and double bonds which then gave rise to additional orientation-dependent intermolecular Coulomb interactions. By adjusting these charges it was possible to obtain an orientational potential consistent with the observed Pa3 structure. Lu, Li, and Martin[17] (LLM) put q and $-2q$ ($q = 0.27e$) point charges at the center of the single and double bonds, respectively. Sprik, Cheng, and Klein[18] (SCK) put charges $q = 0.175e$ on the carbon sites and $-2q$ on the center of double bonds. A detailed study of the lattice dynamics from these potentials can be found in Ref. 15. Even though these potentials give reasonable results for the lattice dynamics of C_{60} concerning the center-of-mass motions, there are problems with their orientational parts. For instance, the LLM potential predicts another minimum in the potential about 100 meV (150 meV if one uses only the Coulomb part of it) above the Pa3 ground-state energy. These values are almost one order of magnitude larger than experimental values. For instance, by inelastic neutron scattering,[19] ultrasonic attenuation,[20] and thermal conductivity measurements,[21] it has been established that the energy difference between these two minima is about 12 meV. (These potentials also predict that these two minima are separated by a potential barrier of 300 meV. This value is indeed in good agreement with the experimental value one deduces from the temperature at which orientational freezing occurs.) The other unpleasant thing about these potentials is that they assume too much charge in the double and single bonds. Quantum-mechanical calculations of electronic wave functions of C_{60} (Refs. 22 and 23) as well as the empirical evidence of bond lengths[24] suggest that the so-called "double" and "single" bonds between carbon atoms in C_{60} are not nearly as different as in other hydrocarbons. For the LLM case, the single bond even has positive charge with respect to carbon sites, which is unphysical. Here we carry out *ab initio* calculations of the electronic charge density based on the local-density approximation (LDA).[25] To the extent that the LLM and SCK potentials give results in agreement with theory, we would view them as being satisfactory ad hoc phenomenological potentials, whose explanation from first principles has yet to be given. The aim of this paper is to give a fundamental discussion of the orientational interactions between C_{60} molecules in the solid state.

Specifically, the first aim of this paper is to verify that currently available intermolecular potentials are unphysical in that they *do not* reflect the actual Coulomb interaction between C_{60} molecules. Thus the statement that the bond charges represent the "small charge transfer between two types of bonds in the C_{60} molecule"[17] is not substantiated by our calculations. To quantify the comparison between the bond charges and the LDA charge density, we first calculate the multipole moments of C_{60} using the quantum-mechanical charge distribution from *ab initio* calculations in two different ways. We then compare these multipoles with those obtained from the point charge models of LLM and SCK. We find that actual values of the lowest moments and Coulomb interaction potential are one order smaller than those predicted from these intermolecular potentials. Consequently, the bond-charge models, although useful in some contexts, cannot be justified from first principles.

Our second aim is to discuss the validity of a multipole expansion for C_{60} in the solid. We show that a multipole expansion including $l = 6$ and $l = 10$ can predict the potential due to a C_{60} molecule for distances (from its center) larger than twice the radius of the C_{60} molecule. For points closer than this distance, but still outside the outer radius of the molecule, the multipole expansion converges only slowly and one must include terms beyond $l = 18$. Since many atoms on a neighboring C_{60} molecule are inside this distance, the multipole expansion is dangerously slowly convergent.

Our last aim is to discuss the Coulomb interactions between C_{60} molecules and to try to answer the following question: "Do Coulomb interactions by themselves stabilize the observed Pa3 structure or not?" For this we first propose a number of point-charge models which all give the correct values of the first five nonzero multipoles of C_{60}. Using these models we show that Coulomb interactions stabilize the Pa3 structure, but with a setting angle $\phi = 93.6°$, in contradiction to the experimental values $\phi = 22°, 26°$.[10,8] This result gives rise to two possibilities: either the multipole expansion is too slowly convergent to be used to describe the $Fm\bar{3}m \rightarrow$ Pa3

transition or an explanation of this transition requires short-range quantum-mechanical interactions. Up to now such short-range interactions have been modeled by the 6-12 Lennard-Jones potential which, as we have mentioned, has the wrong orientational dependence to explain the stability of the observed Pa3 structure. Since the orientational dependence of this potential is comparable to the Coulomb energy we obtain here, one should be careful in modeling the short-range potential by such a Lennard-Jones form. In summary, the orientational interaction between C_{60} molecules consists of the interaction between the static charge distributions on the two molecules which we have calculated here. In addition, there are short-ranged quantum-mechanical repulsive interactions and van der Waals atractive interactions, both of which ought to be calculated from a reliable quantum-mechanical calculation.

Briefly, this paper is organized as follows. In Sec. II we give the details of the calculation of multipole moments. We discuss how (a) the electronic wave functions for the C_{60} molecule are calculated and (b) the integration over the resulting charge density is done to give the multipole moments. In Sec. III we give an alternative determination of the multipole moments using a least-squares fit of the multipole potential to the *ab initio* potential. Comparison of both methods and the validity of the multipole expansion is also discussed in this section. In Sec. IV we discuss previous point-charge models and propose models which more closely reproduce the the multipoles obtained from our *ab initio* calculations. In Sec. V we discuss the Coulomb interaction and the orientational dynamics of C_{60} molecules in solid C_{60} by using point-charge models. Section VI is devoted to the discussion of our results and conclusions.

II. CALCULATION OF THE MULTIPOLES OF C_{60}

A. *Ab Initio* electronic wave functions

In order to evaluate the C_{60} multipole moments, we have computed the electronic charge density $\rho(\mathbf{r})$ and Coulomb potential $\Phi(\mathbf{r})$ directly from ground-state C_{60} wave functions.[22] These wave functions are calculated self-consistently within the framework of the LDA.[25] All electrons are included on equal footing (the pseudopotential approximation is not made), and full orbital relaxation of both core and valence states is allowed. Electron correlation effects are included through the standard LDA treatment, using the Perdew-Zunger parametrization of the Ceperly-Alder exchange-correlation functional.[26] The ground-state geometry predicted by LDA is used here, with hexagonal and pentagonal bond lengths of 1.40 Å and 1.45, Å, respectively.[22]

To solve the Kohn-Sham equations,[25] we have used the linear-combination-of-Gaussian-orbitals cluster code developed at the Naval Research Laboratory by Pederson and Jackson.[27] As described in detail elsewhere,[27] this method takes the one-electron basis functions to be symmetry-adapted combinations of atomiclike orbitals. This set is then supplemented by additional functions to improve the completeness of the basis. The orbitals are expanded on a set of ten Gaussian functions of s and p symmetry, with Gaussian exponents ranging from ~ 0.1 to ~ 4000 bohr^{-2}. A "variational integration mesh" allows direct numerical evaluation, to an arbitrary prescribed tolerance, of the Hamiltonian and overlap matrix elements. Standard diagonalization then leads to an updated charge density and effective potential, and a self-consistent solution is arrived at within about ten iterations.

Once the self-consistent ground-state wave functions have been calculated, the density and potential can be computed on an arbitrary set of points. In the remainder of this paper, $\rho(\mathbf{r})$ will be understood as the density due to the occupied valence states only, although we note again that core states are explicitly included in the self-consistency cycle. As we shall see, the contributions to the multipole moments due to the charge density of the core electrons is conveniently treated. (In our calculation the separation of charge density into "core" and "valence" contributions is a natural one which is easily implemented.) By using a Gaussian basis set, the Coulomb potential (understood to be based on the *total* electron density) can be expressed directly in terms of integrals of the Gaussian functions, bypassing the need for numerical solution of the Poisson equation. The resulting expression for $\Phi(\mathbf{r})$ requires only a one-dimensional integration to evaluate the incomplete γ function, which is easily computed to arbitrary precision.

B. Multipole moments

In this section we describe the calculation of the multipoles of C_{60}. This calculation requires the evaluation of the following three-dimensional integral:

$$Q_l^m = \int_0^\infty r^2 dr \int_0^\pi \sin\theta \, d\theta \int_0^{2\pi} d\phi \, r^l \rho_T(\mathbf{r}) Y_l^{m*}(\theta,\phi) \tag{1}$$

for the multipole Q_l^m of order l. Here, $\rho_T(\mathbf{r})$ is the total charge density of the C_{60} molecule (including core electrons and the positive nuclear charges) and $Y_l^m(\theta,\phi)$ is the spherical harmonic of order l. It is a simple consequence of Gauss's law that outside a spherically symmetric charge distribution the electric fields and potentials are the same as if that charge distribution were concentrated at its center. Since the electronic wave functions we obtain for the core electrons are very close to being spherically symmetric about their atomic centers, we can take account of them by combining the two core electrons on each atom with the six proton charges in the nucleus. Thus $\rho_T(\mathbf{r})$ is replaced by two contributions: one, $\rho(\mathbf{r})$, from the density due to the occupied valence states, and 60 point charges of $+4|e|$ at the carbon nuclei. When applied to interactions between C_{60} molecules, this approximation is an excellent one.

Since by now it has been well established by both NMR (Ref. 4) and neutron experiments[28] that the molecular symmetry of C_{60} in the solid is icosahedral, the nonzero multipoles of C_{60} given in Eq. (1) are $l = 6, 10, 12, 16, 18, \ldots$ and $m = 0, \pm 2, \pm 4, \ldots, \pm l$ with respect to a reference frame in which twofold axes lie along the x, y, and z axes, as shown in Fig. 1(a). The odd m terms are zero because of reflection symmetry. As an alternative to this standard orientation reference frame, it is more convenient to calculate multipoles in a reference frame where a fivefold symmetry axis of C_{60} coincides with the z axis. In this case, the molecule is oriented so that one pentagonal facet is perpendicular to the z axis, as shown in Fig. 1(b). In this frame, because of the fivefold symmetry, Q_l^m vanishes unless m is 0, ± 5, ... Thus, for instance, for $l = 6$ we have only three nonzero multipoles, Q_6^0 and $Q_6^{\pm 5}$. The phase of the complex quantity Q_l^m depends on how the pentagonal facet is oriented, subject to its being in an x'-y' plane. For the choice shown in Fig. 1(b), the x'-z' plane is a reflection plane, and consequently the Q_l^m's are all real. The values given below all refer to this reference frame.

To save computer time and also to increase accuracy in the evaluation of three-dimensional integrals, one can reduce the integration limits given in Eq. (1) using icosahedral symmetry. In our calculations we reduced the integration limits to $0 \leq \theta \leq \pi/2$ and $0 \leq \phi \leq \pi/5$, which results from both inversion and fivefold symmetry of I_h. Note that this region, which is only 1/20 of the entire region, can still be reduced by a factor of 3 because I_h has 120 operations (60 if we omit inversion). What this means is that we are not using the full symmetry. In other words, in our integration region we have three carbon sites and they will be treated independently. Thus our results are unlikely to be consistent with symmetry if they are wrong. On the other hand, if we had used full symmetry, the results would have been guaranteed to be consistent with symmetry whether or not they were correct. Below we will use this fact to provide one check of our results. For the integration of radial distance, we set the limits to $0.5R_0 \leq r \leq 2R_0$ where $R_0 = 3.5485$ Å is the radius of C_{60} molecule. Inclusion of either the larger r or smaller r region does not materially affect the integration because the electron density at these distances goes to zero exponentially. To be precise, we find that only 0.17 (out of 240) electrons lie outside these limits on the radial integration.

Having summarized the reference frame and integration limits used, the contribution to the multipole Q_l^m from the 240 valence electrons is now given by

$$Q_l^m = 20 \int_{0.5R_0}^{2R_0} r^2 dr \int_0^{\pi/2} \sin\theta \, d\theta \times \int_0^{\pi/5} d\phi \, r^l \rho(\mathbf{r}) Y_l^{m*}(\theta, \phi) \, . \tag{2}$$

The contribution to multipoles from the effective core charges of $+4|e|$ on each nucleus can be easily calculated from a single summation over all C atoms and will be added to Q_l^m given in Eq. (2).

Since *ab initio* calculation of $\rho(\mathbf{r})$ can be done efficiently for a large set of points, we first calculated $\rho(\mathbf{r})$ at $43 \times 90 \times 36$ points for $r \times \theta \times \phi$ in the reduced region described above. Then we developed a program to calculate $\rho(\mathbf{r})$ using a spline fit[29] of these points. For the points close to carbon sites [where variation of $\rho(\mathbf{r})$ is large] $\rho(\mathbf{r})$ is calculated from a spline of $31 \times 26 \times 31$ points uniformly distributed in a sphere of radius 0.725 Å centered at the carbon site. The values of the electron density $\rho(\mathbf{r})$ obtained from the spline program described above and from the wave functions directly are identical to within a maximum error of less than 1%. The only remaining difficulty in numerical integration is that the integrand is a fast oscillatory function of the variables θ and ϕ. For this reason, we divide the integration region given in Eq. (2) into $10 \times 10 \times 10$ subintervals. Integration in each subinterval is evaluated to an accuracy of 0.1% requiring, in the worst case, $(250)^3$ function evaluations.

In the first column of Table I we present numerical values of multipoles of C_{60} obtained by direct integration as described above. We also give multipoles from the point-charge models of LLM and SCK. The most im-

TABLE I. Multipoles of C_{60} (in units of $|e|$) obtained from the quantum-mechanical charge distribution and the point-charge models of two recently proposed potential models. Values given in the second and third columns are obtained by 3D integration and a least-squares fit to potential values at 1000 nonequivalent points, respectively. The columns labeled LLM and SCK give the values resulting from the effective point charges in their respective models. The last column shows the ratio between our results and those of LLM for the multipole moments. The values of the multipoles for $m \neq 0$ can be obtained from q_l^0 given here and the ratios Q_l^m/Q_l^0 given in Table II.

$q_l^m = \frac{Q_l^m}{R_0^l}$	9(3 DI)	9(LSQ)	9(LLM)	9(SCK)	$\frac{9(\text{LLM})}{9(3\ \text{DI})}$
q_6^0	0.295	0.285	3.801	1.598	12.88
q_{10}^0	3.550	3.626	1.863	0.202	0.52
q_{12}^0	−0.751	−0.793	−7.320	−3.637	9.75
q_{16}^0	−2.614	−2.431	1.214	−0.854	−0.47
q_{18}^0	22.895	19.997	−0.031	4.790	−0.00135

portant observation is that the first non-zero multipole is approximately 13 times less than that of LLM and 5 times less than the SCK potential. Not surprisingly, as a consequence, the actual Coulomb interaction between C_{60} molecules is much smaller than the values predicted by these potential models. As we show in Sec. IV, this potential does not stabilize the experimentally observed Pa3 structure. Thus the origin of the $Fm\bar{3}m \rightarrow$ Pa3 transition is still not explained on a microscopic level.

The other important observation is that $l = 10$ moment is not small compared to the first nonzero moment $l = 6$. Indeed the contribution to the potential from the $l = 10$ moment at some points is larger than $l = 6$ moment for a distance $r \sim 2R_0$. Note that the potential is proportional to Q_l^m/r^{l+1}. Even though the $l = 18$ moment is large compared to $l = 12$ and $l = 16$, its contribution to the potential is not significant.

In order to check the consistency of our results with the symmetry, we give the ratios Q_l^m/Q_l^0 in Table II both for our calculated values of multipoles and for a general charge density which has icosahedral symmetry. For small l the agreement is fairly good, while the error increases slightly as l increases. The ratios given in the first column of this table are also useful in constructing the symmetry adapted functions of the icosahedral symmetry which transform like the identity. As shown in the Appendix for $l < 30$, we have only one such a function for each l (and therefore only one independent amplitude of the moments for fixed l) and the coefficients of the Y_l^m's were determined numerically as given in Table II.

III. MULTIPOLE EXPANSION

In this section we will discuss an alternative way to determine the values of the multipole moments. In this alternative approach the moments are determined from the values of the Coulomb potential outside the molecule obtained directly from the wave functions, as described in Sec. II A. By fitting this potential to the multipole expansion, the multipole moments can be determined. Comparison of these two approaches indicates that our numerical integrations of the rapidly oscillating spherical harmonics of high order are reasonably accurate.

Before doing this, we have to make sure that the charge distributions of two nearest-neighbor molecules are well separated from each other so that a multipole expansion in the solid phase is valid. In Fig. 2 we plot the sum of the charge densities of the two nearest neighboring molecules as a function of distance along the [110] axis connecting their centers. Solid and dashed lines show the density when both molecules are in their standard orientation and Pa3 orientation, respectively. From this figure we see that the tail of the charge density essentially goes to zero at a distance twice the radius of the C_{60} molecule. Thus we cannot trust the multipole expansion for the points closer than this distance, as we shall see below. The overlap of the charge densities of two nearest-neighboring molecules is small and thus we assume that the charge density of C_{60} in the solid is nearly the same as that of isolated C_{60}. Again from Fig. 2 we see that the amount of charge facing each other along nearest-neighbor direction [110] is reduced by more than a factor of 2 when the molecules are in their Pa3 orientation indicating the importance of Coulomb interaction in the stabilization of Pa3 structure. We shall discuss this in more detail in Sec. IV.

After having justified the validity of the multipole expansion for sufficiently large distances, we express the potential $\Phi(r, \theta, \phi)$ at a point $\mathbf{r} = (r, \theta, \phi)$ due to a C_{60}

TABLE II. Comparison of the calculated ratio of multipole moments with that predicted by symmetry. The third column shows the ratio $\left(\frac{Q_l^m}{Q_l^0}\right)$ of the multipoles of any charge distribution which has icosahedral (I_h) symmetry. The last column shows the same ratios for the calculated values of the multipoles which are given in the first column of Table I.

l	m	$\left(\frac{Q_l^m}{Q_l^0}\right)$ (icosahedral)		$\left(\frac{Q_l^m}{Q_l^0}\right)$ (Calc.)
6	5	$\left(\frac{7}{11}\right)^{1/2} \sim$	0.80	0.82
10	5	$-\left(\frac{33}{13}\right)^{1/2} \sim$	−1.59	−1.61
10	10	$\left(\frac{187}{247}\right)^{1/2} \sim$	0.87	0.86
12	5	$\left(\frac{286}{1071}\right)^{1/2} \sim$	0.52	0.51
12	10	$\left(\frac{247}{357}\right)^{1/2} \sim$	0.83	0.83
16	5	$-\left(\frac{663}{1216}\right)^{1/2} \sim$	−0.74	−0.65
16	10	$-\left(\frac{271}{301}\right)^{1/2} \sim$	−0.95	−0.86
16	15	$\left(\frac{601}{1110}\right)^{1/2} \sim$	0.74	0.70
18	5	$\left(\frac{125}{393}\right)^{1/2} \sim$	0.56	0.58
18	10	$\left(\frac{379}{1857}\right)^{1/2} \sim$	0.45	0.47
18	15	$\left(\frac{861}{1084}\right)^{1/2} \sim$	0.89	0.93

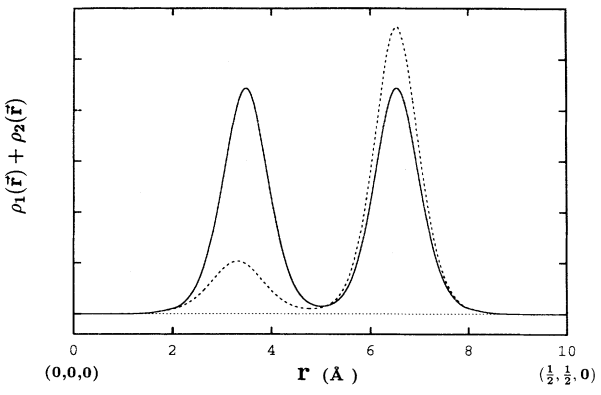

FIG. 2. Charge density of two nearest-neighbor C_{60} molecules along [110] directions (in arbitrary units). The solid and dashed lines show the density when both molecules are in their standard and Pa3 orientations, respectively. Here (0,0,0) is the location of sublattice 1, as defined in Ref. 15, and (1/2,1/2,0) to sublattice 4. The small maximum at about 3.5 Å corresponds to passing through an electron-poor region of a pentagonal face. The large maximum at about 6.5 Å corresponds to passing through an electron-rich region of a double bond.

molecule by the following multipole expansion:

$$\Phi(r,\theta,\phi)=\sum_{l=0}^{\infty}\frac{4\pi}{2l+1}\frac{Q_l^0}{r^{l+1}}\sum_{m=-l}^{l}\left(\frac{Q_l^m}{Q_l^0}\right)Y_l^m(\theta,\phi). \quad (3)$$

As discussed in the Appendix, for each $l<30$ the ratio $\left(\frac{Q_l^m}{Q_l^0}\right)$, given in Table II, is the same for all charge distributions having I_h symmetry. Thus for $l<30$ we have only one unknown Q_l^0. So, if we know the potential $\Phi(\mathbf{r})$ at many points, we can make a least-squares fit with respect to Q_l^0 in Eq. (3). The best fit should be obtained at the values of Q_l^0 found in Sec. II.

The function that we are going to minimize is

$$R(Q_6^0,...,Q_l^0)=\frac{1}{N}\sum_{i=1}^{N}\left(\frac{\Phi(\mathbf{r}_i)-\Phi_q(\mathbf{r}_i)}{\Phi_q(\mathbf{r}_i)}\right)^2. \quad (4)$$

Here N is the number of points used in the fit and $\Phi_q(\mathbf{r})$ is the potential at point $\mathbf{r}$ obtained by quasianalytical integration of charge density, as discussed in Sec. II A. The function R is the average fractional error per point. We terminate the l summation in Eq. (3) at $l=18$ and minimize R with respect to variables Q_l^0 for $l=6,10,12,16$, and 18. We used many different sets of 1000 inequivalent points and the results did not vary significantly. For the points where $r\le\frac{3}{2}R_0$, it is not possible to predict the potential using the multipole expansion given in Eq. (3). We do not even get the sign right. This means that one should worry about quantum-mechanical effects at these distances. For distances $r\ge 2R_0$ the multipole expansion works very well and by including only $l=6$ and $l=10$ one can predict the potential due to a C_{60} molecule within an error about 5%. Inclusion of higher-order terms up to $l=18$ reduces this error to 2.8%. In the second column of Table I we give the values of Q_l^m at which the function R in Eq. (4) is minimized for many different set of 1000 inequivalents points. These values agree with the values found by direct integration method, as shown in first two columns of Table I. This agreement suggests that our numerical integrations are reasonably accurate.

IV. POINT-CHARGE MODELS FOR C_{60}

In this section we shall discuss possible point-charge models for the charge distribution of a C_{60} molecule which reproduce the calculated multipoles. Such a model will be very useful in the calculation of the crystal potential energy and other relevant properties. By now only two point-charge models have been proposed. In Sec. III we have seen that both models predict wrong values for the multipoles and thus are not satisfactory. The major assumption in both models is that there is a large charge difference between single and double bonds. This assumption is not correct, as one can see from Fig. 3. In this figure we show the charge density along double and single bonds and along paths from a carbon site through the center of hexagon and pentagon. While the charge density at the double and single bonds are almost the same it is remarkably low at the center of hexagons and pentagons. Thus one should try to simulate the charge density by putting positive charges at these electron deficiency regions as we shall do in model II.

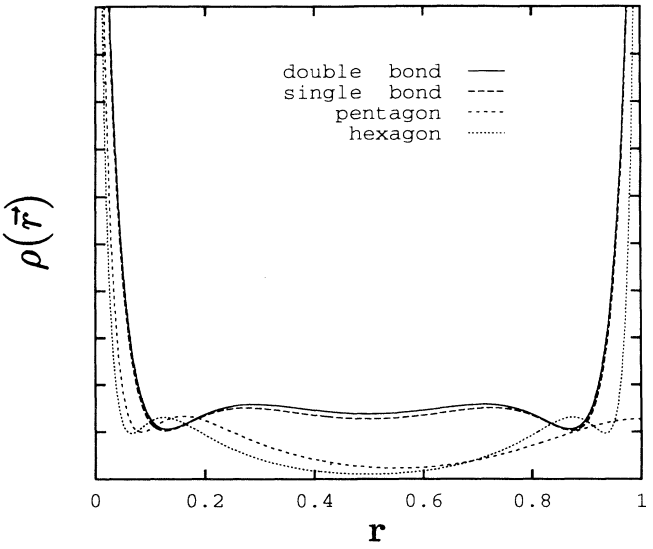

FIG. 3. The solid and long-dashed lines give the charge density of C_{60} along single and double bonds, respectively, as a function of the fractional distance r along the bond. Note that the charge densities of single and double bonds do not differ appreciably. The short-dashed and dotted lines give the charge density along a path which starts at a carbon site and ends across the plaquette at another carbon site (for the hexagon) and at the center of a double bond (for the pentagon). Note that the charge density at the center of the hexagon or pentagon is quite small.

As discussed in Sec. III, the multipole expansion does not converge at distances $r\le\frac{3}{2}R_0$, indicating that one should not hope to model the actual charge distribution of C_{60} by a simple point-charge model. We shall see this below more clearly.

A. Model I

In this model we shall try to simulate the charge density of C_{60} by three different point charges q_C, q_S, and q_D located on a carbon site and somewhere on the single and double bonds, respectively. We assume that the fractional distance of q_S and q_D from a carbon site is, respectively, R_S and R_D. Figure 4(a) shows a schematic representation of this charge distribution. This model is capable of reproducing the LLM model for $R_D=R_S=0.5$, $q_C=0$, $q_D=-2q_S$ and the SCK model for $R_D=R_S=0.5$, $q_S=0$, $q_D=-2q_C$. However, as we shall see below, such a model cannot produce the values of the multipoles of C_{60} that we have calculated.

Before fixing the parameters R_D, R_S, q_C, q_S, and q_D so that multipoles from this model will be same as those calculated in Sec. II, it is useful to discuss the physical regions for the values of the parameters. The fractional

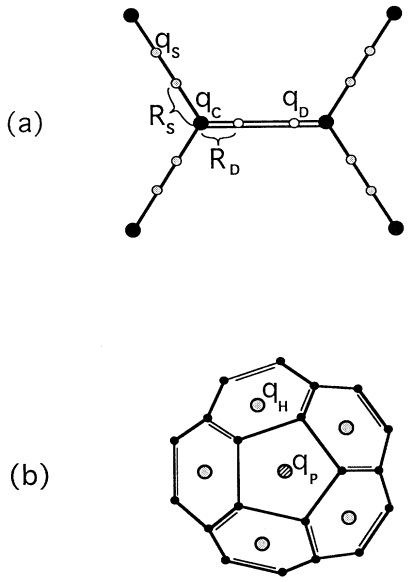

FIG. 4. (a) Positions of the point charges on the single and double bonds for the point-charge model I. In the text, it is shown that from this model it is not possible to fit the first five nonzero multipoles of C_{60} by simply varying the distances R_S and R_D. (b) Location of additional positive charges at the center of hexagons and pentagons in model II.

distances R_D and R_S are restricted to lying between 0 and 0.5. The charge q_C on the carbon site should be positive and less than +4 if we assume that two core electrons are spherically distributed on the C nucleus. The bond charges q_S and q_D must be negative. Furthermore, since C_{60} is neutral, the charges must be satisfy the constraint

$$q_C + q_D + 2q_S = 0. \tag{5}$$

The multipole Q_l^m arising from this model is given by

$$Q_l^m = q_C S_{lm}^C(0) + q_S S_{lm}^S(R_S) + q_D S_{lm}^D(R_D), \tag{6}$$

where

$$S_{lm}^\alpha(R_\alpha) = \sum_{i\in\alpha} r_i^l Y_l^m(\theta_i, \phi_i), \quad \alpha = C, S, D. \tag{7}$$

From this equation and the constraint in Eq. (5), we see that for a given R_S and R_D, we have a 2×2 set of linear equations. Thus using the calculated values of Q_l^m for two different l, we can fix q_C, q_S, and q_D. We have solved the set of linear equations in Eq. (6) for 50×50 values of R_S and R_D in the interval [0, 0.5] and unfortunately *could not* get any physical solution as described above. We find that q_C is always negative and q_S and q_D are positive to get correct values for multipoles of order $l = 6$, 10. Therefore we have explicitly shown that it is impossible to model the charge density of C_{60} by this model which includes both the LLM and the SCK potentials.

Before giving up this model, it may be useful to discuss the following point. Since at large and small distances from the center of the C_{60} molecule the charge distribution is almost spherically distributed, this part of the charge distribution can be represented by putting a negative charge ϵ at the center of C_{60}. Since at these distances the wave function is very small, ϵ should be small. Thus the total charge on the C_{60} molecule $q_C + q_D + 2q_S$ given in Eq. (5) no longer needs to be zero. It can be slightly positive. Since now we have no constraint, Eq. (6) becomes a 3×3 set of linear equations and can be solved using calculated values of Q_l^m for $l = 6, 10$, and 12. Unfortunately, the solution of this equation for 50×50 values of R_S and R_D in the interval [0,0.5] always gives positive ϵ rather than negative, indicating that this model and others based on the difference in the charges of single and double bonds are unphysical, and thus we abandon them.

B. Model II

In Sec. IV A we have seen that the difference between double and single bonds is not enough to model the actual charge density of the C_{60} molecule. Here we propose another point-charge model which uses the fact that the anisotropic charge distribution of the C_{60} molecule actually originates from the electron deficiency around the center of hexagons and pentagons.[10,30] In order to support this idea, in Fig. 3 we show the charge densities along double and single bonds and along a path through the center of hexagons and pentagons. Note that charge densities along double and single bonds are almost the same[22–24] while there are electron deficiencies around the center of hexagons and pentagons. Thus one may think of the charge density of C_{60} as a spherically distributed cloud of valence electrons, denoted q_0, *plus* positive charges q_P and q_H at the center of pentagons and hexagons to create electron deficiency [see Fig. 4(b)]. The distances from the center of C_{60} to q_H and q_P are denoted by R_H and R_P, respectively. (In other words, these plaquette charges are not required to lie in the plane of the hexagonal or pentagonal face.) We have of course again q_C core charges at the carbon sites. To create electron-rich double and single bonds with respect to the spherically symmetrically distributed charge q_0, we will again put point charges q_S and q_D at the fractional distances R_S and R_D on single and double bonds, respectively. From the charge neutrality of C_{60} we have

$$q_0 + 60q_C + 120q_S + 60q_D + 20q_H + 12q_P = 0, \tag{8}$$

where the charge q_0 is put at the center of the molecule.

Since we have five independent point charges in this model, we can fit all multipoles up to $l = 18$. Because of the free parameters R_S, R_D, R_H, and R_P we do not have unique solutions. However, no matter which solution we use, we get the same potential energy because all solutions give the same values for the first five nonzero multipoles and higher orders do not have much effect on the potential. We expect q_C, q_P, and q_H to be positive.

TABLE III. Different solutions for the point-charge model II which reproduce the calculated values of the first five nonzero multipoles of C_{60}. $R_0 = 3.5485$ Å is the radius of C_{60}. All charges are given in units of $|e|$. (So q_0 is always negative, whereas q_H and q_P are always positive.)

R_D	R_S	R_H	R_P	q_C	q_D	q_S	q_H	q_P	q_0
0.3		$0.870R_0$	$1.031R_0$	0.675	− 0.277	0	3.218	0.688	−96.496
0.5[a]	0.5[a]	$0.962R_0$	$1.078R_0$	0.435	− 0.324	−0.147	0.739	0.237	− 6.644
0.5[a]	0.2	$0.962R_0$	$1.031R_0$	0.829	− 0.373	−0.353	0.736	0.375	− 4.220

[a]At this value of R_D and R_S, two charges along the bond converges to the center of bond and thus we have $2q_D$ and $2q_S$ charges at the double and single bond centers, respectively.

In Table III, we list a few solutions. The first solution is the one which contains a minimum number of point charges. The other solutions include more point-charge centers, but do not have any advantage over the first solution. When we set both $q_D = q_S = 0$ we do not get any physical solutions to fit the five multipoles. However, by varying R_H and R_P one can fit the moments $l = 6, 10$, and 12. The model with $q_S = q_D = 0$ has 93 point charges on a C_{60} molecule and predicts the potential with an error twice that of the model with nonzero bond charges, which has 153 effective charges.

V. INTERMOLECULAR COULOMB INTERACTION IN SOLID C_{60}

After having presented the values of multipoles and point-charge models for C_{60} we can now discuss the interaction between C_{60} molecules in solid arising from the charge distribution of C_{60}. Since the point-charge models proposed in Sec. IV give the first five nonzero multipoles of C_{60} correctly, the Coulomb interaction can be well approximated by the interaction of point charges located on the C_{60}. Thus the Coulomb interaction between molecules I and J is

$$V_{IJ} = \sum_{i\in I}\sum_{j\in J} q_i q_j / R_{ij}, \tag{9}$$

where i, j runs over the effective charges of each molecules given in Table III. In our calculations we use the set of charges as given in the first row of Table III, since it has fewer interaction centers than others.

We show various contributions to the total potential energy as a function of setting angle ϕ in Fig. 5. Molecules in each sublattice are rotated about their [111] directions starting from the standard orientation ($\phi = 0$). In order to make comparison between different models we show the Lennard-Jones potential, the LLM point-charge model, and our multipole model in Figs. 5(a), 5(b), and 5(c), respectively. The first thing we notice is that the potential energy from the multipole expansion is about ten times less than that from LLM. Thus when our multipole interaction is used, the orientational dependence of the 12-6 potential will become important in the selection of the ground state. Note that the Lennard-Jones potential has its global minimum at around $\phi \sim 80°$ and thus does not by itself stabilize the observed Pa3 structure. Aside from the disagreement in magnitudes of the LLM model and our multipole model, the two potentials are qualitatively very similar up to $\phi \sim 70°$. For the setting angle $\phi > 70°$ a strong disagreement between the two potentials appears. While our model gives the global minimum at $\phi \sim 93°$, the LLM potential predicts a *maximum* near this angle (the same is true for the SCK potential). This difference is a direct consequence of the particular assignment of point charges in the two earlier models.

To get more insight into the meaning of the various potentials, we show, in Fig. 6, the potential energy of a molecule at the origin when it is rotated through an angle Θ about the local threefold axis of symmetry relative to its equilibrium value in the Pa3 structure, when all other molecules are held in their ground-state orientations, taken with $\phi = 23.3°$. This potential energy would determine the nature of the lowest branch[15] of librational excitations if it were legitimate to consider them as being localized. (Librons are nearly localized, since their energy depends only weakly on wave vector.) In the top panel of Fig. 6 we show the contributions to this potential from the Lennard–Jones and the bond-charge model of LLM separately. (The results for the SCK potential are similar to those of the LLM potential.) We see that in these models the libron dynamics for excitations near the ground state are dominated by the Coulomb interactions due to the bond charges. The libron frequencies (which depend on the curvature of the potential near its minimum), the barrier height, and the difference in energy between the two minima are all dominated by these bond-charge interactions. All these quantities are much smaller when the potential is taken to be the sum of the Lennard-Jones term and the multipole potential. The multipole potential is plotted in the bottom panel of Fig. 6. This potential by itself does have the two expected minima, one is at $\Theta = 0°$ and the other at $\Theta = 60°$. Their energy difference is 2.2 meV, which is smaller than the experimental value 12 meV.[19–21] However, the Coulomb part of the LLM potential and the SCK potential both predict an energy difference between these two minima of about 150 meV. A difference of this magnitude seems implausible to us, as we now discuss. As pointed out by David and co-workers,[10,30,19] the Pa3 structure ($\Theta = 0$ in Fig. 6) has the center of a pentagon of one molecule facing a double bond. This configuration is favorable because these regions correspond to low and high electron densities, respectively. However, nearly the same argument also applies when the double bond faces the center of a hexagon, as it does when $\Theta \approx 60°$. Thus these two

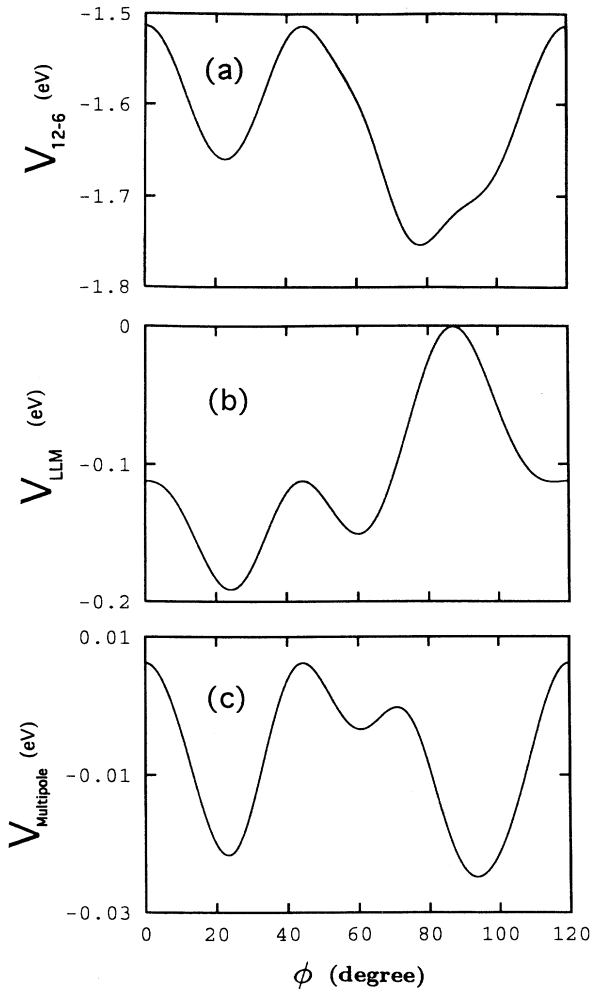

FIG. 5. Variation of the potential energy with setting angle ϕ, i.e., each molecule is rotated about its [111] threefold axis (see Ref. 15) for various potentials. (a) Lennard-Jones atom-atom potential with parameters given in Ref. 17, (b) bond-charge interaction in the model of LLM, and (c) Coulomb interaction using model II (with parameters taken from the first row of Table III) for the location of the point charges. Insignificant differences arise from the other models of Table III.

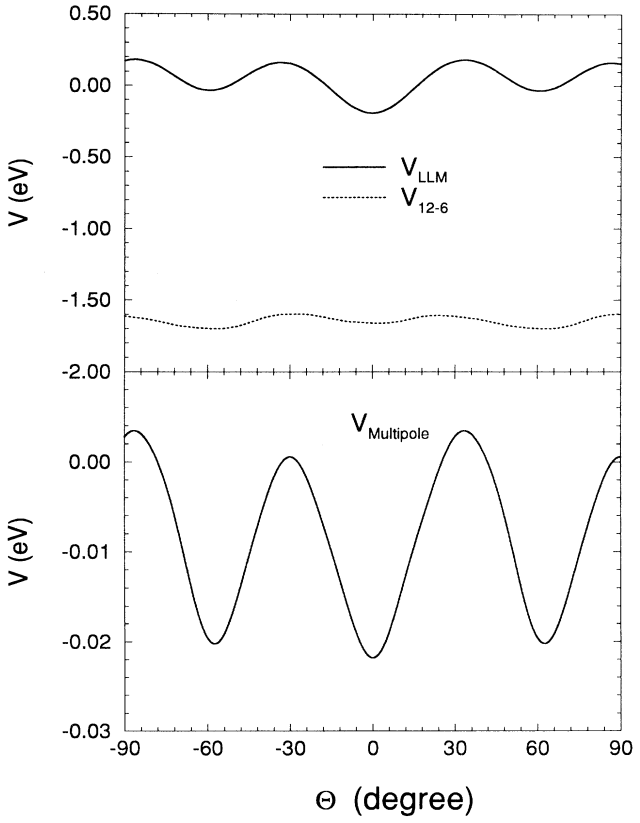

FIG. 6. The potential energy for a C_{60} molecule located at (0,0,0) as a function of rotation angle Θ, away from its Pa3 orientation, when all other molecules are held in their ground-state orientations with the setting angle $\phi = 23.3°$. The bond-charge model of Lu, Li, and Martin (V_{LLM}) and Lennard-Jones ($V_{12\text{-}6}$) potential energies are plotted as a solid line and a dotted line, respectively, in the top panel. The bottom panel is a similar plot using only the multipole potential.

configurations should be close in energy as predicted by the multipole potential as shown in the bottom panel of Fig. 6. However, one sees that the LLM potential gives a large energy difference between these two configurations as shown in the top panel of Fig. 6. The reason for this large energy difference is that in the LLM model the pentagon carries a total charge $+5q$ on its bonds, whereas the hexagon carried a total charge $-3q$ on its bonds. Thus in the bond-charge models there is a big difference between pentagons and hexagons. In contrast, within the LDA pentagons and hexagons are rather similar. That the experiments show a smaller value (12 meV) for the relative energy of the metastable minimum at $\Theta \sim 60°$ than that (150 meV) given by the LLM potential may be taken as evidence in support of the multipole potential.

Although our model is successful in predicting a local minimum in the potential at the observed Pa3 structure, the global minimum corresponds to a Pa3 structure with the setting angle $\phi = 93.6°$; this is in contradiction to experimental observations. We note, however, that our multipole potential predicts this structure to be only 3 meV lower in energy than the experimentally observed $\phi = 23.3°$. Potential differences of this magnitude may well be at or near the limits of convergence of our multipole expansion. Thus more complete calculations are required, incorporating a more realistic treatment than a simple multipole expansion for the Coulomb interaction between C_{60} molecules.

Since the global mimimum in Coulomb interactions we find corresponds to a Pa3 with the wrong setting angle, there must be another mechanism that causes the observed transition $Fm\bar{3}m \rightarrow$ Pa3. The most likely candidate for this is the short-range interaction between C_{60}

molecules which has been modeled by the 12-6 potential, but which, by itself, does not stabilize the observed Pa3 structure. However, in combination with the multipole interaction, another form of this short-range repulsive interaction might possibly stabilize the observed Pa3 structure. Of course the other possibility (which we consider unlikely) is that the charge distribution of C_{60} in the solid is much different than one of isolated C_{60}, which we used in our calculations. Such a possibility would require the careful treatment of overlap integrals between nearest-neighboring C_{60} molecules.

VI. CONCLUSION

We have studied the orientational dependence of the Coulomb interaction between C_{60} molecules by means of a multipole expansion based on the quantum-mechanical charge density of C_{60} from *ab initio* calculations. In summary we have reached the following conclusions.

(1) We calculated the first five nonzero multipoles (l = 6–18) of C_{60} in two different ways. We showed the second nonzero multipole ($l = 10$) is not small compared to the $l = 6$ moment and thus one has to keep (at least) both terms in order to obtain the electrostatic potential due to a C_{60} molecule. The multipole expansion converges very slowly for the points close to C_{60} but still outside the charge distribution and requires the inclusion of the terms beyond $l = 18$.

(2) The first nonzero moment and Coulomb interaction based thereon was shown to be one order smaller than the values from phenomenological potentials previously proposed by Lu, Li, and Martin[17] and by Sprik, Cheng, and Klein.[18]

(3) We showed that it is not possible to simulate the charge density of C_{60} by a point-charge model which is based only on the differences between double and single bonds. It is essential to also put positive point charges on the center of hexagons and pentagons to create electron-poor regions as pointed out David *et al.*[10] We proposed a model of effective point charges which reproduces the first five nonzero moments of C_{60}.

(4) In particular, our model II, which incorporates the charge deficiency in hexagons and pentagons, predicts two minima which are close to each other in energy as expected from simple qualitative arguments[10,19] unlike the Lu-Li-Martin and the Sprik-Cheng-Klein potentials. However, the global minimum corresponds to a Pa3 structure with wrong setting angle $\phi = 93.6°$. This discrepancy is due to either (a) the fact that the multipole expansion does not converge fast enough to predict correctly the sign of the small energy difference between these two minima or (b) the failure of the Lennard-Jones potential to accurately represent the short-range repulsive quantum interactions between molecules. As is well known, the Lennard-Jones potential, by itself, does not stabilize the observed Pa3 structure.[16]

(5) The electrostatic interaction obtained here can also play a role in understanding the structure of M_3C_{60} and other doped systems. This study will be reported elsewhere.[31]

ACKNOWLEDGMENTS

We acknowledge helpful conversations with E. J. Mele and R. Sachidanandam. A.B.H. and T.Y. were supported in part by the National Science Foundation under Grant No. NSF-91-22784. We also acknowledge partial support from the National Science Foundation under the MRL program, Grant No. DMR88-19885. Some of the computations were supported by a grant from the Research Foundation of the University of Pennsylvania. S.C.E. was supported in part by the Laboratory for Research on the Structure of Matter (University of Pennsylvania). M.R.P. was supported in part by the Office of Naval Research.

APPENDIX: MULTIPOLE AMPLITUDES

In this appendix we obtain the number of independent amplitudes necessary to specify the $(2l + 1)$ multipole moments of degree l. One can address this question as follows. The $(2l + 1)$ spherical harmonics $Y_l^m(\theta, \phi)$ provide a basis for a $(2l + 1)$-dimensional representation of the icosahedral group. In general this representation is reducible and will contain each irreducible representation Γ of the icosahedral group $g_\Gamma(l)$ times. In particular, the one-dimensional identity representation E is contained $g_E(l)$ times in the $(2l + 1)$-dimensional representation. Thus there are $g_E(l)$ linear combinations of the Y_l^m's which are invariant under all the operations of the icosahedral symmetry group. This number can also be identified as the number of independent amplitudes required to specify the Q_l^m's.

We determine g_E by[32]

$$g_E(l) = \frac{1}{60} \sum_R \chi_I(R)\chi_l(R) , \tag{A1}$$

where R is one of the 60 operations of the icosahedral group, $\chi_I(R)$ is the character of R for the identity representation of icosahedral group, and $\chi_l(R)$ is the character of R for the $(2l+1)$-dimensional representation in the spherical harmonic basis. There are five classes of operators, the indentity operator E, and the various rotations through an angle θ corresponding to twofold, threefold, and fivefold rotations. The corresponding characters for the identity representation are

$$\chi_I(E) = 1 , \quad \chi_I(\pi) = 1 , \quad \chi_I(2\pi/3) = 1 , \quad \chi_I(2\pi/5) = 1 , \quad \chi_I(4\pi/5) = 1 . \tag{A2}$$

To calculate characters in the spherical harmonic basis, it is convenient to choose a coordinate system in which the rotations are always taken about the z axis. Thus the character is obtained as the trace of the $[(2l+1)\times(2l+1)]$-dimensional transformation matrix. In this way we find[32]

$$\chi_l(E) = 2l + 1 , \quad \chi_l(\theta) = \frac{\sin\{[l + (1/2)]\theta\}}{\sin[(1/2)\theta]} , \tag{A3}$$

Taking account of the number of operators in each class[33] we get the explicit result

$$g_E(l) = \frac{1}{60}\left[2l+1+15\frac{\sin\{[l+(1/2)]\pi\}}{\sin(\pi/2)}+20\frac{\sin[(2l+1)\pi/3]}{\sin(\pi/3)}+12\frac{\sin[(2l+1)\pi/5]}{\sin(2\pi/5)}+12\frac{\sin[(4l+2)\pi/5]}{\sin(4\pi/5)}\right], \quad \text{(A4)}$$

from which it follows that $g_E(l)$ first becomes larger than 1 for $l = 30$: $g_E(30) = 2$.

[1] A. F. Hebard, M. J. Rosseinsky, R. C. Haddon, D. W. Murphy, S. H. Glarum, T. T. M. Palstra, A. P. Ramirez, and A. R. Kortan, Nature **350**, 600 (1991).

[2] H. S. M. Coxeter, *Regular Polytopes*, 3rd ed. (Dover, New York, 1973), p. 52.

[3] H. W. Kroto, J. R. Heath, S. C. O'Brien, R. F. Curl, and R. E. Smalley, Nature **318**, 162 (1985).

[4] C. S. Yannoni, R. D. Johnson, G. Meijer, D. S. Bethune, and J. R. Salem, J. Phys. Chem. **95**, 9 (1991).

[5] K. Hedberg, L. Hedberg, D. S. Bethune, C. A. Brown, H. C. Dorn, R. D. Johnson, and M. D. Vries, Science **254**, 410 (1991).

[6] P. A. Heiney, J. E. Fischer, A. R. McGhie, W. J. Romanow, A. M. Denenstein, J. P. McCauley Jr., and A. B. Smith III, Phys. Rev. Lett. **66**, 2911 (1991).

[7] R. M. Fleming, T. Siegrist, P. M. March, B. Hessen, A. R. Kortan, D. W. Murphy, R. C. Haddon, R. Tycko, G. Dabbagh, A. M. Mujsce, M. L. Kaplan, and S. M. Zahurak, in *Clusters and Cluster-Assembled Materials*, edited by R.S. Averback, J. Bernholc, and D. L. Nelson, MRS Symposia Proceedings No. 206 (Materials Research Society, Pittsburgh, 1991), p. 691.

[8] R. Sachidanandam and A. B. Harris, Phys. Rev. Lett. **67**, 1467 (1991).

[9] P. A. Heiney, J. E. Fischer, A. R. McGhie, W. J. Romanow, A. M. Denenstein, J. P. McCauley, A. M. Smith III, and D. E. Cox, Phys. Rev. Lett. **67**, 1468 (1991).

[10] W. I. F. David, R. M. Iberson, J. C. Matthewman, K. Prassides, T. J. S. Dennis, J. P. Hare, H. W. Kroto, R. Taylor, and D. R. M. Watton, Nature **353**, 147 (1991).

[11] S. Liu, Y.-J. Lu, M. M. Kappes, and J. A. Ibers, Science **254**, 408 (1991).

[12] A. B. Harris and R. Sachidanandam, Phys. Rev. **46**, 4944 (1992).

[13] K. H. Michel, J. R. D. Copley, and D. A. Neumann, Phys. Rev. Lett. **68**, 2929 (1992).

[14] X.-P. Li, J. P. Lu, and R. M. Martin, Phys. Rev. B **46**, 4301 (1992).

[15] T. Yildirim and A. B. Harris, Phys. Rev. B **46**, 7878 (1992).

[16] Y. Guo, N. Karasawa, and W. A. Goddard III, Nature **351**, 464 (1991).

[17] J. P. Lu, X.-P. Li, and R. M. Martin, Phys. Rev. Lett. **68**, 1551 (1992).

[18] M. Sprik, A. Cheng, and M. L. Klein, J. Phys. Chem. **96**, 2027 (1992).

[19] K. Prassides, H. W. Kroto, R. Taylor, D. R. M. Walton, W. I. F. David, J. Tomkinson, M. J. Rosseinsky, D. W. Murphy, and R. C. Haddon, Carbon (to be published).

[20] X. D. Shi, A. R. Kortan, J. M. Williams, A. M. Kini, B. M. Savall, and P. M. Chaikin, Phys. Rev. Lett. **68**, 827 (1992).

[21] R. C. Yu, N. Tea, M. B. Salamon, D. Lorents, and R. Malhotra (unpublished).

[22] M. R. Pederson and A. A. Quong, Phys. Rev. B **46**, 13 584 (1992).

[23] B. P. Feuston, W. Andreoni, M. Parrinello, and E. Clementi, Phys. Rev. B **44**, 4056 (1991).

[24] Quantum calculations, such as those done here or in Refs. 22 and 23, give bond lengths of 1.40 and 1.45 Å, in agreement with experiment (Refs. 4 and 5). Normal bond lengths of carbon-carbon double and single bonds are, respectively, about 1.34 and 1.53 Å as given by both LDA calculations [M.R. Pederson, K.A. Jackson, and W.E. Pickett, Phys. Rev. B **44**, 3891 (1991).] and experiment; see *Handbook of Chemistry and Physics* (CRC, Boca Raton, FL, 1992).

[25] P. Hohenberg and W. Kohn, Phys. Rev. **136**, B864 (1964); W. Kohn and L. J. Sham, *ibid.* **140**, A1133 (1965).

[26] J. P. Perdew and A. Zunger, Phys. Rev. B **23**, 5048 (1981).

[27] M.R. Pederson and K. A. Jackson, Phys. Rev. B **41**, 7453 (1990); **43**, 7312 (1991); K. A. Jackson and M. R. Pederson, *ibid.* **42**, 3276 (1990).

[28] P. C. Chow, X. Jiang, G. Reiter, P. Wochner, S. C. Moss, J. D. Axe, J. C. Hanson, R. K. McMullan, R. L. Meng, and C. W. Chu, Phys. Rev. Lett. **69**, 2943 (1992).

[29] Carl de Boor, *A Practical Guide to Splines* (Springer-Verlag, New York, 1978).

[30] W. I. F. David, R. M. Ibberson, T. J. S. Dennis, J. P. Hare, and K. Prassides, Europhys. Lett. **18**, 219 (1992).

[31] T. Yildirim, S. Hong, A. B. Harris, and E. J. Mele (unpublished).

[32] M. Tinkham, *Group Theory and Quantum Mechanics* (McGraw-Hill, New York, 1964).

[33] T. C. Lubensky, in *Introduction to Quasicrystals*, edited by M. V. Jarić (Academic, New York, 1988), pp. 199 and 238.